Fossil insect eyes shed light on trilobite optics and the arthropod pigment screen

Lindgren, Johan; Nilsson, Dan Eric; Sjövall, Peter; Jarenmark, Martin; Ito, Shosuke; Wakamatsu, Kazumasa; Kear, Benjamin P.; Schultz, Bo Pagh; Sylvestersen, René Lyng; Madsen, Henrik; LaFountain, James R.; Alwmark, Carl; Eriksson, Mats E.; Hall, Stephen A.; Lindgren, Paula; Rodríguez-Meizoso, Irene; Ahlberg, Per

Published in:
Nature

DOI:
10.1038/s41586-019-1473-z

2019

"This is the peer reviewed version of the following article: Lindgren et al. 2019: Fossil insect eyes shed light on trilobite optics and the arthropod pigment screen. Nature 573, 122-125., which has been published in final form at https://www.nature.com/articles/s41586-019-1473-z.

Fossil insect eyes shed light on trilobite optics and the arthropod pigment screen

Johan Lindgren[1], Dan-Eric Nilsson[2], Peter Sjövall[3], Martin Jarenmark[1], Shosuke Ito[4], Kazumasa Wakamatsu[4], Benjamin P. Kear[5], Bo Pagh Schultz[6], René Lyng Sylvestersen[6], Henrik Madsen[7], James R. LaFountain Jr.[8], Carl Alwmark[1], Mats E. Eriksson[1], Stephen A. Hall[9], Paula Lindgren[1], Irene Rodríguez-Meizoso[10] & Per Ahlberg[1]

[1]Department of Geology, Lund University, 223 62 Lund, Sweden. [2]Department of Biology, Lund University, 223 62 Lund, Sweden. [3]RISE Research Institutes of Sweden, Chemistry and Materials, 501 15 Borås, Sweden. [4]Department of Chemistry, Fujita Health University School of Health Sciences, Toyoake, Aichi 470-1192, Japan. [5]Museum of Evolution, Uppsala University, 752 36 Uppsala, Sweden. [6]Museum Salling, Fur Museum, 7884 Fur, Denmark. [7]Museum Mors, Mo-clay Museum, 7900 Nykøbing Mors, Denmark. [8]Department of Biological Sciences, University at Buffalo, Buffalo, New York 14260, USA. [9]Department of Construction Sciences, Lund University, 223 63 Lund, Sweden. [10]Centre for Analysis and Synthesis, Department of Chemistry, Lund University, 221 00 Lund, Sweden.

Fossilized eyes permit inferences of visual capacity in extinct arthropods[1–3]. However, structural and/or chemical modifications resulting from taphonomic and diagenetic processes can alter the original features, necessitating comparisons with modern species. Here we report the detailed molecular composition and microanatomy of 54-million-year-old crane-fly eyes, which provide a proxy for interpreting optical systems in some other ancient arthropods. These well preserved visual organs comprise calcified corneal lenses that are separated by intervening spaces containing eumelanin pigment. We also show that eumelanin is present in the facet walls of living crane-flies, where it forms the outermost ommatidial pigment shield in a chitinous cornea. This is the first record of melanic screening pigments in arthropods, and reveals a novel fossilization mode in insect eyes involving a decay-resistant biochrome coupled with early diagenetic mineralization of the ommatidial lenses. Such demonstrable secondary calcification of an initially chitinous lens cuticle has implications for the proposed calcitic corneas of trilobites, which we posit are preservational artefacts rather than a product of *in vivo* biomineralization[4–7]. Thus, while trilobite eyes might have been partly mineralized for mechanical strength, a more likely organic composition would have enhanced function via gradient-index optics and increased control of lens shape.

Arthropod compound eyes are the most common visual organs found in the animal kingdom[8], and have an evolutionary history extending back at least 520 million years (Myr) to the early Cambrian[1,2,9]. They comprise large numbers of regularly arranged visual units termed ommatidia, each of which incorporates a cuticular facet and a cluster of photoreceptor cells surrounded by screening pigment cells[10]. Dark biochromes (natural pigments) shield the photoreceptor cells from light entering the ommatidia from outside of the visual field[10]. Most animals utilize melanins for this purpose; however, there is as yet no evidence for their existence in arthropod eyes[11,12]. Instead, extant insects, arachnids, myriapods and crustaceans all employ ommochromes (and to some extent carotenoids and pterines) to both shield and filter light[11–14].

In contrast to melanins, which have been well-documented in the fossil record[15,16], recognizable geochemical traces of ommochromes have hitherto not been detected. Here we therefore use a series of molecular and ultrastructural analyses to characterize both a residual pigment and the microanatomy of crane-fly eyes from the earliest Eocene (~54 Myr ago) Fur Formation of Denmark (see Supplementary Information). We experimentally compare these with optic tissues from living crane-flies to determine how the fossilization process has affected the conservation of compound eyes through deep time.

The marine diatomaceous deposits of the Fur Formation are replete with insect fossils, most of which are preserved as high-fidelity compressions showing varying degrees of disarticulation[17]. Crane-

flies (Tipuloidea) are usually represented by detached wings, although virtually complete individuals have also been recovered. Collectively, the accumulated material records a diverse assemblage comprising over a dozen species attributable to three family-level groupings: Tipulidae, Limoniidae and Cylindrotomidae[18,19].

Twenty-three crane-fly fossils with exceptionally preserved compound eyes were excavated specifically for this investigation (Fig. 1 and Extended Data Fig. 1). These specimens were not treated with preservatives or consolidants, and have been accessioned into the collections at Museum Salling (FUM) and Mo-clay Museum (MHM) in Denmark. Four fossils were split along their long axis to produce opposing part and counterpart sections, while the others are represented by part sections only. All of the Fur Formation crane-flies are herein classified as indeterminate tipulids pending a more detailed taxonomic assessment.

The remnant compound eyes occur as darkly coloured, ovate to sub-triangular structures with sharply defined edges (Fig. 1a and Extended Data Fig. 1). Wrinkles and folds are visible along their perimeters (Extended Data Fig. 1b, d—arrowheads), suggesting an originally non-biomineralized composition comparable to that of extant crane-fly eyes[20]. At higher magnification, the visual surfaces consist of a honeycomb of repeated identical units representing the outermost (corneal) portion of the hexagonal ommatidia (Fig. 1b, c and Extended Data Fig. 1b, d, f, h). Field emission gun scanning electron microscopy (FEG-SEM) with energy-dispersive X-ray spectroscopy (EDS) established that the corneal facet walls are composed of a dense fine-grained substance (Extended Data Fig. 1l) that is enriched in carbon, but with minor amounts of sulfur and nitrogen (Extended Data Fig. 2). Imaging microanalysis further revealed that each facet houses a single lens-shaped body (about 30 μm in diameter) with a convex distal surface (Extended Data Fig. 1i) and concave proximal termination (Fig. 1d and Extended Data Fig. 1j). Internally, the fossilized lenses contain a homogeneous crystalline material that is exposed in broken sections where the outermost surface has been sheared off (Fig. 1e and Extended Data Fig. 1k). Calcium, oxygen and magnesium are co-localized within these mineralized structures (Fig. 2a, b and Extended Data Fig. 2), implying diagenetic replacement of both the corneal exo- and endocuticle by magnesium-containing calcite. In addition, electron back-scatter diffraction (EBSD) measurements demonstrated that the calcite crystals are arranged with their *c*-axis perpendicular to the optical surface (Fig. 2c and Extended Data Fig. 3).

The calcitic composition of the fossilized lenses was independently verified by time-of-flight secondary ion mass spectrometric (ToF-SIMS) analysis. Mass spectra obtained directly from the lens interiors (exposed when the plane of splitting passes tangentially through the visual surface) were dominated by mineral-derived ions, mainly $(CaO)_n^+$ and $Ca(CaO)_n^+$ peaks, consistent with calcium carbonate (Fig. 2d and Extended Data Fig. 4).

ToF-SIMS was also employed to examine the molecular composition of the corneal facet walls, with the acquired spectra compared against an array of compounds including synthesized and artificially degraded samples of the ommochrome xanthommatin (see Supplementary Information). However, rather than correlating with this biochrome, the fossil spectra showed closest agreement (both in intensity distribution and peak positions) with those obtained from our eumelanin control samples (Fig. 3 and Extended Data Figs. 4k, 5, 6); although spectral differences between xanthommatin and eumelanin reduced upon maturation (Extended Data Fig. 6).

To substantiate this unexpected finding of a molecular species with spectral consistency to eumelanin, samples of our fossil crane-fly eyes were subjected to alkaline hydrogen peroxide oxidation (AHPO), which is an assay expressly developed for the detection of eu- and pheomelanins via the production of discrete chemical markers that serve to quantify the melanin content of pigmented tissues[16,21]. AHPO recovered low but measurable amounts (Table 1) of pyrrole-2,3,5-tricarboxylic acid (PTCA), pyrrole-2,3-dicarboxylic acid (PDCA) and pyrrole-2,3,4,5-tetracarboxylic acid (PTeCA), with a PTeCA/PTCA ratio (4.07) comparable to previously documented ancient eumelanins (see Supplementary Information).

Furthermore, we investigated the composition of the ommatidial pigment shield in the modern tiger crane-fly, *Nephrotoma suturalis*. Chemical isolates from the compound eyes of approximately 1,300 laboratory raised adult individuals were obtained via purification methods that included mechanical and enzymatic degradation, as well as solvent extraction (see Supplementary Information). Notably, the hexagonal corneal facet walls containing the intracuticular pigmentation remained

morphologically intact throughout these processing procedures (Extended Data Fig. 7), attesting to their tough structural and/or molecular composition.

The isolates then underwent AHPO treatment and hydriodic acid (HI) reductive hydrolysis, resulting in the retrieval of considerable quantities of breakdown products from the corneal facet walls specific to DOPA- and dopamine(DA)-derived eumelanins (Table 1). AHPO thus verifies the presence of this biochrome in the outermost tipulid ommatidial pigment shield (Fig. 1h—'Pigmented facet walls'), a conclusion that was supported by both ToF-SIMS analysis (Fig. 3e and Extended Data Fig. 8) and histochemical staining (Extended Data Fig. 9).

Our discovery of eumelanin in corresponding examples of a fossil and living insect contradicts the widely accepted hypothesis that melanic screening pigments are absent in arthropod compound eyes[11,12,22]. Moreover, we show that this biochrome is diffusely incorporated into the cuticle between the facet lenses (Fig. 1g, h), rather than being housed within specialized cellular organelles (melanosomes) as otherwise occurs in the eyes of most other animals including vertebrates, flatworms and cnidarians (see also Supplementary Information)[11,12,22,23].

Our inability to detect equivalent molecular traces of ommochromes in the fossil crane-flies, together with the apparent sensitivity of these pigments to experimental degradative treatments, imply that they are unlikely to survive across geological time. We therefore propose that the dark colouration occasionally seen in the head region of other fossil arthropods (e.g. refs. 17, 24) also represents residual eumelanins.

The Fur Formation crane-fly eyes further evince that the originally chitinous corneal lenses were replaced by single calcium carbonate crystals that have their *c*-axis aligned along the optical axis of each ommatidium (Fig. 2c and Extended Data Fig. 3). An identical condition occurs in the compound eyes of trilobites (Extended Data Fig. 10), an iconic group of extinct marine arthropods[4–7]. Numerous studies have reconstructed the possible optical properties of calcite lenses in trilobites[5–7,25], but failed to identify any obvious functional advantages relative to the chitinous and proteinaceous lenses otherwise ubiquitous in extant arthropods. Instead, a completely mineralized cornea would have posed major complications including image blurring due to birefringence, as well as difficulties in obtaining an optimal lens shape, and the need to gradually modify the lens curvature during ontogeny, or otherwise re-grow new calcite lenses during each exoskeletal molt. A predominantly chitinous cornea, on the other hand, would suffer none of these issues and additionally allow for graded index optics[10,26]. Although aragonite lenses have been reported in living polyplacophoran molluscs (chitons)[27], these form part of an external shell that does not undergo cyclical molting and permits only low resolution vision with limited precision. Conversely, the much more demanding optics of crane-fly and trilobite compound eyes render extensive *in vivo* mineralization of an initially organic cornea highly unlikely. Nonetheless, it is conceivable that trilobite corneas were partly mineralized in life for mechanical strength, which is similar to the condition seen in many extant crustaceans (Extended Data Fig. 10n and Supplementary Information)[28,29]. Yet, our recognition of secondarily calcified lenses in a fossil insect strongly infers that their now completely inorganic composition can be more feasibly interpreted as a product of taphonomic and/or diagenetic processes rather than natural selection. This is supported by the fact that trilobite eyes (as well as those of other ancient arthropods) are frequently replicated by different minerals, including calcium phosphate and iron oxide (limonite), when these are abundant in the surrounding sediments[2,9,30]. Thus, we conclude that the long-standing hypothesis of calcitic corneas in trilobites requires reconsideration, and that the composition and optic properties of their compound eyes instead should be viewed as akin to those of modern arthropods in being primarily organic.

Table 1 | Melanin markers in corresponding examples of fossil and extant crane-fly compound eyes.

	AHPO (μg/mg)					HI hydrolysis (μg/mg)		
Sample	PTCA	PDCA	PTeCA	TTCA	TDCA	4-AHP	4-AHPEA	3-AHPEA
Fossil crane-fly eyes	3.04×10^{-3}	0.59×10^{-3}	12.30×10^{-3}	0.00×10^{-3}	0.00×10^{-3}	-	-	-

Nephrotoma complete eyes	0.17	0.17	0.085	0.68	0.11	0.005	0.045	0.013
Nephrotoma corneas	0.65	0.57	0.39	0.03	0.01	-	-	-
Nephrotoma facet walls #1	1.51	1.49	0.70	< 0.20	< 0.10	0.01	0.12	0.04
Nephrotoma facet walls #2	1.70	1.33	1.12	< 0.10	< 0.10	0.04	0.15	0.05
Nephrotoma facet walls (extract)	0.81	0.45	0.58	0.00	0.00	-	-	-
Nephrotoma sub-corneal pigment #1	0.05	0.08	0.13	5.25	1.97	0.00	0.35	0.03
Nephrotoma sub-corneal pigment #2	0.04	0.02	0.00	3.13	0.24	0.00	0.21	0.02

The fossil crane-fly eyes were analysed four times independently, which yielded similar results. The complete *Nephrotoma* eyes were subjected to AHPO twice independently with similar results, and once using HI hydrolysis. All other samples were analysed once.

Online content
Any methods, additional references, Nature Research reporting summaries, source data, statements of data availability and associated accession codes are available at…

1. Lee, M. S. Y. *et al*. Modern optics in exceptionally preserved eyes of Early Cambrian arthropods from Australia. *Nature* **474,** 631–634 (2011).
2. Paterson, J. R. *et al*. Acute vision in the giant Cambrian predator *Anomalocaris* and the origin of compound eyes. *Nature* **480,** 237–240 (2011).
3. Anderson, R. P., McCoy, V. E., McNamara, M. E. & Briggs, D. E. G. What big eyes you have: the ecological role of giant pterygoid eurypterids. *Biol*. *Lett*. **10,** 20140412 (2014).
4. Towe, K. M. Trilobite eyes: calcified lenses in vivo. *Science* **179,** 1007–1009 (1973).
5. Gál, J., Horváth, G., Clarkson, E. N. K. & Haiman, O. Image formation by bifocal lenses in a trilobite eye? *Vis*. *Res*. **40,** 843–853 (2000).
6. Schoenemann, B., Clarkson, E. N. K. & Horváth, G. Why did the UV-A-induced photoluminescent blue-green glow in trilobite eyes and exoskeletons not cause problems for trilobites? *PeerJ* **3,** e1492 (2015).
7. Schoenemann, B. & Clarkson, E. N. K. Vision in fossilised eyes. *Trans*. *R*. *Soc*. *Edinburgh*, *Earth Environ*. *Sci*. **106,** 209–220 (2017).
8. Land, M. F. & Nilsson, D.-E. *Animal Eyes* (Oxford University Press, 2002).
9. Schoenemann, B., Pärnaste, H. & Clarkson, E. N. K. Structure and function of a compound eye, more than half a billion years old. *Proc. Natl. Acad. Sci.* **114,** 13489–13494 (2017).
10. Nilsson, D.-E. & Kelber, A. A functional analysis of compound eye evolution. *Arthropod Struct*. *Develop*. **36,** 373–385 (2007).
11. Vopalensky, P. & Kozmik, Z. Eye evolution: common use and independent recruitment of genetic components. *Phil*. *Trans*. *R*. *Soc*. *B* **364,** 2819–2832 (2009).
12. Clements, T. *et al*. The eyes of *Tullimonstrum* reveal a vertebrate affinity. *Nature* **532,** 500–503 (2016).
13. Ziegler, I. Genetic aspects of ommochrome and pterine pigments. *Adv*. *Gen*. **10,** 349–403 (1961).
14. Struwe, G., Hallberg, E. & Elofsson, R. The physical and morphological properties of the pigment screen in the compound eye of a shrimp (Crustacea). *J*. *Comp*. *Physiol*. **97,** 257–270 (1975).
15. Lindgren, J. *et al*. Molecular preservation of the pigment melanin in fossil melanosomes. *Nat*. *Commun*. **3,** 824 (2012).
16. Glass, K. *et al*. Direct chemical evidence for eumelanin pigment from the Jurassic Period. *Proc*. *Natl*. *Acad*. *Sci*. **109,** 10218–10223 (2012).
17. Pedersen, G. K. *et al*. Moleområdets geologi – sedimenter, fossiler, askelag og glacialtektonik. *Geologisk Tidsskrift* **2011,** 41–135 (2011).

18. Freiwald, A. Insekten aus der Fur-Formation von Dänemark (Moler, ob. Paleozän/unt. Eozän?). 4. Tipulidae. *Meyniana* **42,** 47–63 (1990).
19. Krzemiński, W. New fossil Tipuloidea (Diptera) from the Fur Formation of Denmark in the collection of the Natural History Museum in London. *Polish J. Entomol*. **70,** 333–339 (2001).
20. Williams, D. S. Organisation of the compound eye of a tipulid fly during the day and night. *Zoomorphologie* **95,** 85–104 (1980).
21. Ito, S. *et al*. Usefulness of alkaline hydrogen peroxide oxidation to analyse eumelanin and pheomelanin in various tissue samples: application to chemical analysis of human hair melanins. *Pigm. Cell Melanoma Res*. **24,** 605–613 (2011).
22. Oakley, T. H. & Speiser, D. I. How complexity originates: the evolution of animal eyes. *Ann. Rev. Ecol. Evol. Syst*. **46,** 237–260 (2015).
23. Needham, A. E. *The Significance of Zoochromes* (Springer-Verlag, 1974).
24. Ren, D., Shih, C., Gao, T., Yao, Y. & Zhao, Y. *Silent Stories – Insect Fossil Treasures from Dinosaur Era of the Northeastern China* (Science Press, 2010).
25. Clarkson, E., Levi-Setti, R. & Horváth, G. The eyes of trilobites: the oldest preserved visual system. *Arthropod Struct. Develop*. **35,** 247–259 (2006).
26. Nilsson, D.-E. in *Facets of vision*. 30–73 (Springer-Verlag, 1989).
27. Speiser, D. I., Eernisse, D. J. & Johnsen, S. A chiton uses aragonite lenses to form images. *Curr. Biol*. **21,** 665–670 (2011).
28. Alagboso, F. I., Reisecker, C., Hild, S. & Ziegler, A. Ultrastructure and mineral composition of the cornea cuticle in the compound eyes of a supralittoral and a marine isopod. *J. Struct. Biol*. **187,** 158–173 (2014).
29. Fabritius, H.-O. *et al*. Functional adaptation of crustacean exoskeletal elements through structural and compositional diversity: a combined experimental and theoretical study. *Bioinspir. Biomim*. **11,** 055006 (2016).
30. Ahlberg, P., Szaniawski, H., Clarkson, E. N. K. & Bengtson, S. Phosphatised olenid trilobites and associated fauna from the Upper Cambrian of Västergötland, Sweden. *Acta Palaeontol. Pol*. **50,** 429–440 (2005).

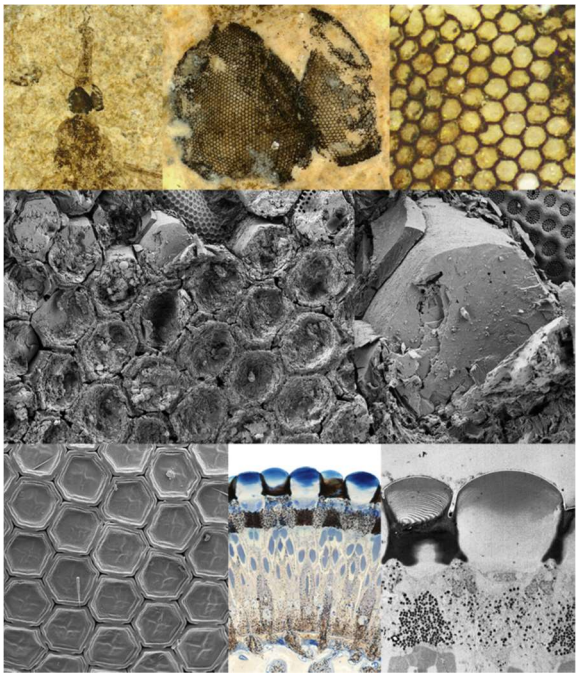

Figure 1 | Structure of fossilized crane-fly compound eyes. a, Cephalic region of FUM-N-13923 (immersed in Milli-Q water) in bedding-plane view showing well-defined eyes preserved as dark stains. **b**, Enlargement of the paired compound eyes illustrating the regularly arranged hexagonal ommatidial facets. **c**, Magnification of the organically preserved corneal facet walls and mineralized ommatidial lenses (**a**–**c**; *n* = 23

fossils). **d**, FEG-SEM micrograph of the boxed area in **c** showing the concave proximal termination of the fossilized ommatidial lenses. **e**, Magnification of a tangentially broken and somewhat corroded ommatidial lens (**d**, **e**; *n* = 4). Fw, facet wall. **f**, FEG-SEM micrograph of ommatidia in a compound eye of the extant tiger crane-fly, *Nephrotoma suturalis* (*n* = 2 specimens). The collapsed appearance of the lens surfaces is an artefact of the FEG-SEM preparation. **g**, Histological section through the ommatidia in *N. suturalis* (*n* = 11 animals). **h**, TEM micrograph of the cornea and underlying cellular structures in *N. suturalis* (*n* = 5). Pigm fw, pigmented facet walls; Pigm gran, pigment granules. Scale bars, 10 μm (**e**, **h**), 30 μm (**d**, **f**), 50 μm (**c**, **g**), 300 μm (**b**), 2 mm (**a**).

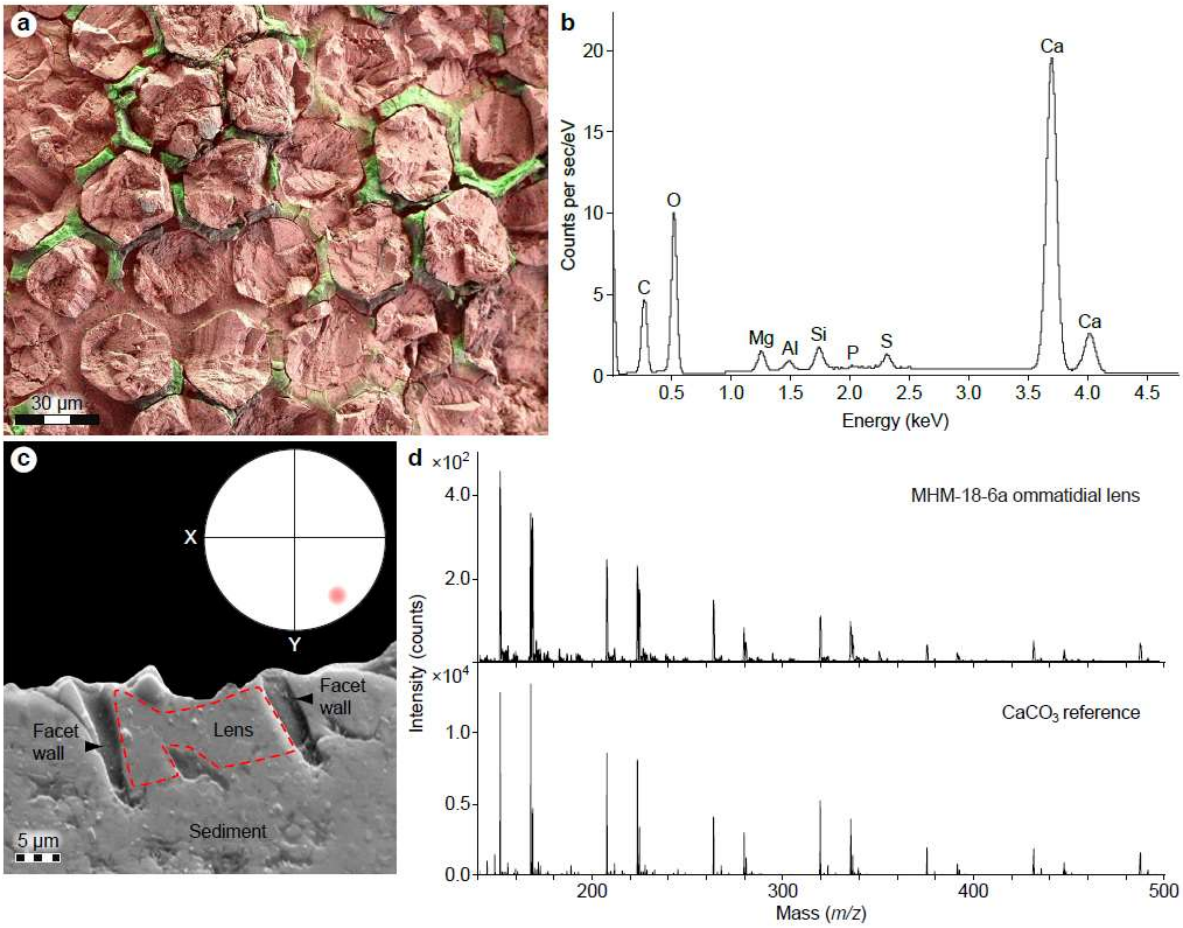

Figure 2 | Chemistry of fossilized crane-fly ommatidial lenses. a, Semi-transparent single-element EDS maps of calcium (red) and carbon (green) superimposed onto a FEG-SEM micrograph of the transversely sectioned cornea in MHM-18-6a (*n* = 3 analyses; see also Extended Data Fig. 2). **b**, Single spot EDS spectrum obtained from the centre of an ommatidial lens in FUM-N-13923. Appreciable intensities of calcium, carbon and oxygen are consistent with calcite. Data are representative of three independent measurements. **c**, Oblique vertical section through a mineralized ommatidial lens from FUM-N-13923 (stippled red line demarcates the analysed area). Inset pole figure (stereographic projection, upper hemisphere) illustrates the orientation of the {0001} (*c*-axis) of the single calcite crystal (*n* = 15 separate lenses; see also Extended Data Fig. 3). **d**, Positive ion ToF-SIMS spectrum acquired from a fossilized ommatidial lens in MHM-18-6a (*n* = 6 measurements) compared against a calcium carbonate reference sample (*n* = 3 measurements). Note close spectral agreement with pronounced peaks from $Ca(CaO)_n^+$ (*n* = 1, 2, 3, 4, 5, 6) and $(CaO)_n^+$ (*n* = 2, 3, 4, 5, 6, 7). Scale bars, 5 μm (**c**), 30 μm (**a**).

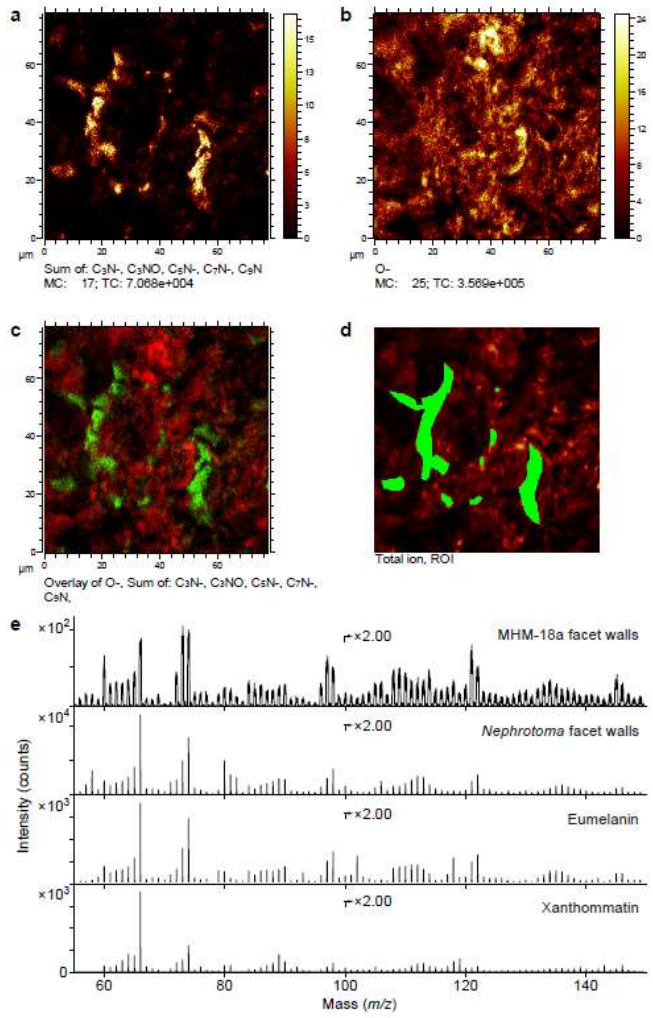

Figure 3 | Chemistry of fossilized crane-fly corneal facet walls. a–**d**, Negative ion ToF-SIMS data from one of the eyes in MHM-18a showing the spatial distribution of **a**, eumelanin-related ions (added signal intensities from C_3N^-, C_3NO^-, C_5N^-, C_7N^- and C_9N^-) and **b**, oxygen (O^-, mainly representing calcite; see Fig. 2d and Extended Data Fig. 4l), together with **c**, a two-colour overlay image where eumelanin-derived ions are marked in green and oxygen in red, and **d**, the total ion image where regions of interest (green) used to generate the 'MHM-18a facet walls' spectrum in **e** are indicated (**a**–**d**; *n* = 6 measurements). **e**, Negative ion ToF-SIMS spectra derived from (top to bottom) the corneal facet walls in MHM-18a (*n* = 6 measurements), the corneal facet walls in the extant tiger crane-fly, *Nephrotoma suturalis* (*n* = 3 measurements), a natural (*Sepia*) eumelanin reference (*n* = 3 measurements) and the synthetic ommochrome xanthommatin (*n* = 3 measurements). Although the main peaks in the eumelanin spectrum also occur in xanthommatin, the relative signal intensity distribution of these ions in spectra from the extant and fossil crane-fly corneal facet walls more closely correlates with eumelanin than xanthommatin (see also Extended Data Figs. 6, 8).

METHODS

Fossil material. The fossil crane-flies were prepared mechanically, before being wrapped in aluminium foil and kept isolated within sealed containers until examined. Fresh aluminium foil was used to cover all work areas, and surgical gloves were worn during all handling and treatment of the specimens. Identical experimental conditions were employed for the fossil and comparative extant materials, but these samples were kept strictly segregated in separate laboratory spaces at all times.

Extraction and purification of modern screening pigments. The extant tiger crane-fly (*Nephrotoma suturalis*) compound eyes (n = 1,300 male and female adults collected 2–7 days after emergence from pupae) were initially washed in acetone, ethyl acetate and Milli-Q water, before being suspended in Milli-Q water prior to grinding and extraction of soluble components. This process was repeated until the extracts were colourless, and the remaining corneas freed from adhering debris. The corneas were then sequentially and repeatedly treated with multiple proteases and a chitinase under argon (Table 1—'*Nephrotoma* facet walls #1'), following methods adapted from Novellino *et al*.[31]. The samples were subsequently washed in heptane and incubated in concentrated HCl(aq) for 24 h, before being rinsed in Milli-Q water and dried under a stream of argon(g). Approximately 7 mg (dry weight) of the corneal facet wall pigment was thus finally isolated and collected (Table 1—'*Nephrotoma* facet walls #2').

Aqueous extracts from the grinding process were treated with butanol and methanol to precipitate proteins, and then filtered before sulfurous acid was added to precipitate the extractable sub-corneal pigment(s) as a dark red solid with a dry weight of 9.6 mg (Table 1—'*Nephrotoma* sub-corneal pigment #1').

Extractions were also undertaken on complete eyes using formic acid (Table 1—'*Nephrotoma* sub-corneal pigment #2'), and the remaining corneas (Table 1—'*Nephrotoma* corneas') treated with 1M NaOH(aq) without prior exposure to enzymes. The facet wall pigment was then precipitated from the supernatant by adding 35% HCl(aq). Purification involved repeated dissolution in 2M NaOH(aq) and re-precipitation with 35% HCl(aq), which ultimately isolated a brownish solid (Table 1—'*Nephrotoma* facet walls (extract)').

Synthesis of xanthommatin and melanins. We followed the protocols of Butenandt *et al*.[32] to synthesize xanthommatin. However, to avoid contamination from trace amounts of phosphate and sulfate salts (which interfered with the ToF-SIMS analysis), all of our re-crystallizations were undertaken in inert atmospheric conditions using degassed solutions of NaOH(aq), HCl(aq) and methanol, as opposed to potassium phosphate-buffers, sulfurous acid or SO_2 gas. Our synthesis of DOPA, cysteinyldopa (from 1:1 molar ratio of DOPA and cysteine), 5,6-dihydroxyindole, dopamine (DA), and cysteinyldopamine (from 1:1 molar ratio of DA and cysteine) melanins employed the methodology of d'Ischia *et al*.[33]. Natural pheomelanin was extracted and purified from the cheek feathers of 4–11-month-old male zebra finches, *Taeniopygia guttata* (n = 16), using the protocol developed by Novellino *et al*.[31].

Maturation experiments. Selected samples and standards were placed in aluminum foil capsules and autoclaved in a stainless-steel high-pressure vessel (30 × 10 mm column, Applied Porous Technologies) connected to an argon gas cylinder. The autoclave was first purged three times by filling it to 80 bar with argon gas, and then to approximately 75% of the desired final pressure before heating at 250 °C in a thermostat-controlled oven (GC oven, 5890 series II, Hewlett Packard). After the system had thermally equilibrated, the pressure was adjusted to 200 bar and the samples matured for 24 or 72 h.

Light microscopy (LM). Adult *Nephrotoma suturalis* were decapitated, and the heads immersed in a fixative solution (consisting of 2.5% glutaraldehyde/2% paraformaldehyde/2% sucrose/5mM EGTA in 0.1M sodium cacodylate buffer, pH 7.3) at 4 °C for 48 h. They were then rinsed multiple times in a sodium cacodylate buffer, and post-fixated for 1 h in 1% OsO_4 diluted in dH_2O at 4 °C. The heads were subsequently rinsed in sodium cacodylate buffer, before being dehydrated in a graded ethanol series, rinsed in acetone, and finally infiltrated with epoxy resin (Agar 100, Resin kit R1031) for 12 h prior to embedment in fresh epoxy and curation for 48 h at 60 °C. Semi-thin (2-µm) sections were then cut using a RMC PT-X ultramicrotome and collected onto chrome alum gelatine-coated glass microscope slides, before being stained with methylene blue/Azure II dye for a few sec. The stained sections were rinsed in water and dried on a hotplate before final mounting with clean coverslips. The thin sections were viewed on an Olympus CX21LED microscope equipped with a Nikon DC-Fi1c digital camera.

Our fossil samples were examined untreated on an Olympus SZX16 microscope equipped with an Olympus SC30 camera.

Polarized light microscopy. Compound eye remains from one fossil crane-fly (FUM-N-13923), together with four well-preserved comparative examples of trilobites (LO 12437t–LO 12440t; Department of Geology, Lund University, Sweden), were embedded in a clear polyester resin

(Araldite DBF) to prevent shattering during slide preparation. Thin sections were then cut using a slow-speed diamond saw, before being fixed to petrographic slides with polyester resin, and ground to optical translucency. The polished sections were inspected on an Olympus BX51 polarizing microscope equipped with a UC30 Olympus 3.2 MP digital camera.

We also used comparative modern samples comprising compound eyes from three freshly excised adult (precise age and sex unknown) sandy swimming crabs, *Liocarcinus depurator*. The corneas were removed and mechanically freed from adhering soft tissue. They were then placed on microscope slides in drops of sea water, and coverslips were applied. The micrograph in Extended Data Fig. 10n was taken under crossed polarizers using a Zeiss polarizing microscope with a 10× objective.

Field emission gun scanning electron microscopy (FEG-SEM), energy-dispersive X-ray (EDS) and electron back-scatter diffraction (EBSD) microanalysis. The fossil crane-flies were first coated with platinum/palladium using a Cressington 208HR High Resolution Sputter Coater. They were then examined in a Tescan Mira3 High Resolution Schottky FEG-SEM fitted with both standard and in-lens secondary electron, as well as back-scattered electron detectors; these were set at acceleration voltages of 1–15 kV and a working distance of 3–15 mm. Elemental analyses and mappings were performed with a linked energy-dispersive spectrometer (X-MaxN 80, 124 eV, 80 mm^2) from Oxford Instruments.

Additional gold/palladium-coated (15-nm) samples were examined using a Zeiss Supra 40VP FEG-SEM set at 1 keV electron energy and a working distance of 3–6 mm (Everhart-Thornley secondary electron detector). Elemental analyses and mappings employed a X-Max 50 mm^2 silicon drift detector (SSD) from Oxford Instruments with 15 keV electron energy and a working distance of 8–9 mm.

EBSD measurements were taken on an electron back-scatter diffraction spectrometer (NordlysNano, Oxford Instruments, Aztec HKL software) linked to a Tescan Mira3 High Resolution Schottky FEG-SEM. One of the fossil crane-flies, FUM-N-13923, was cut and polished to EBSD standard using colloidal silica, before being coated with 5 nm carbon. The EBSD data were acquired with a working distance of 15 mm, 20 keV under high vacuum, 4 × 4 binning, and a high gain setting to optimize patterns. The step size was set to 0.5–2 µm with automatic indexing of Kikuchi bands performed using the standard hexagonal unit cell parameters for calcite (space group R-3c: a = 4,990 Å, c = 17,061 Å). The EBSD data were subsequently processed on the Channel 5 software package (Oxford Instruments) with a single wild-spike correction to remove noise. The results were visualized as orientation maps with the inverse pole figure colouring scheme, and as pole figures (stereographic projection, upper hemisphere) to show the orientation of the data points in relation to the fossilized ommatidial lenses. The pole figures were correlated with both the LM and FEG-SEM images to determine the orientation of the plane {0001}, and thus the calcite *c*-axis, in relation to each individual lens.

Transmission electron microscopy (TEM). *Nephrotoma suturalis* compound eyes were fixed and embedded in epoxy resin as described above. Ultra-thin sections (50-nm) were then cut on a RMC PT-X ultramicrotome equipped with a diamond knife, and mounted on pioloform-coated copper grids before staining with 2% uranyl acetate and lead citrate. The sections were finally examined on a JEOL JEM-1400 PLUS TEM at 100 kV. Micrographs were recorded with a JEOL Matataki CMOS camera using TEM Centre for JEM1400 Plus software.

X-ray computed microtomography. X-ray computed microtomography was performed on a Zeiss XRadia XRM520. An X-ray tube voltage of 80 kV was used with a source power of 7 W. The applied tube voltage resulted in a broad spectrum of X-ray energies; the manufacturer-supplied Le4 source filter was applied to reduce beam hardening effects, and gave an effective energy of the spectrum of 36.8 keV. The resulting cone-beam provides a geometrical magnification of the image depending on the source-detector distance and the position of the sample between the two; the sample was therefore placed with the centre of rotation at 12.51 mm from the source, and at 26.65 mm from the detector. Optics after the scintillator gave a magnification of 4×. Three thousand two hundred and one radiographs (2,032 × 2,032 pixels) were acquired over 360° with an exposure time of 5 sec for each image. The subsequent tomographic reconstruction, using the Zeiss reconstructor software (XradiaReconstructorApp V11.0) with correction for the centre of rotation, provided cubic voxels with

side lengths of 1 µm. The resulting 16-bit tiff-images were processed and analysed using the Voxler 3 software package.

Time-of-flight secondary ion mass spectrometry (ToF-SIMS). The fossil crane-flies were mounted on ToF-SIMS sample holders without prior treatment, whereas our comparative materials (in particle form) were attached to silicon substrates using double-sided tape. ToF-SIMS analyses were conducted in the static SIMS mode on a TOFSIMS IV instrument (IONTOF GmbH) using 25 keV Bi_3^+ primary ions and low energy electron flooding for charge compensation. Positive and negative ion data were acquired with instrument optimization for either high mass-resolution (m/Δm ~5,000, spatial resolution ~3–4 µm) or high image-resolution (m/Δm ~300, spatial resolution ~0.2–0.5 µm) because these properties cannot be optimized simultaneously without an inordinate increase in analysis time[34]. The pulsed primary ion current was set at 0.10 pA for the high mass-resolution data, and 0.04 pA for the high image-resolution data.

We also undertook ToF-SIMS analyses on synthetic and natural variants of eumelanin (both untreated and experimentally matured samples), pheomelanin, pyomelanin, and several porphyrins (see details in refs. 15, 35, 36). We additionally examined other comparative materials including calcium carbonate (Merck), chitin (Sigma) and synthetic xanthommatin (both untreated and experimentally matured samples; see Supplementary Information), as well as screening pigments isolated from the eyes of *Nephrotoma suturalis* (see Supplementary Information).

Principal component analysis (PCA) of negative ion ToF-SIMS spectra was performed with the Solo software (Eigenvector Research Inc.), and included all major eumelanin peaks in the mass range *m/z* 48–146 (see Supplementary Information). In addition, all main pheomelanin peaks in this same mass range were also evaluated (Extended Data Fig. 8). Peak intensities were normalized to the total added signal intensity of the included peaks, and the data pre-processed via mean centering and Poisson scaling. Ion image PCA (Extended Data Fig. 5) was conducted using the SurfaceLab 6.8 software (ION-TOF GmbH) on images of negative ions between *m/z* 10 and *m/z* 150 (141 images in total).

Alkaline hydrogen peroxide oxidation (AHPO). Our experiments utilized 0.1 mg (100 µl of 10 mg/ml suspension) of synthetic pigments, 0.8–1.3 mg of eyes, extracted biochromes and corneas from *Nephrotoma suturalis* (see Supplementary Information), and 10–12 mg of fossil crane-fly eye material (the latter substrate was treated with 6M HCl prior to analysis[37]). All samples were subjected to AHPO following the protocol established by Ito *et al*.[21]: 100 µl water, 375 µl 1M K_2CO_3 and 25 µl 30% H_2O_2 were added to each test tube. After vigorous mixing at 25 °C for 20 h, the residual H_2O_2 was decomposed via the addition of 50 µl 10% Na_2SO_3, and the resulting mixture acidified with 140 µl 6M HCl. The oxidation mixture was then centrifuged at 10,000*g* for 1 min, and an aliquot (80 µl) of the supernatant injected directly into a high-performance liquid chromatography (HPLC) system. The setup comprised a JASCO 880-PU liquid chromatograph (JASCO Co.), a Shiseido C18 column (Capcell Pak, Type MG; 4.6 × 250 mm; 5 µm particle size; Shiseido) and a JASCO UV detector monitored at 269 nm. The mobile phases included 0.1M potassium phosphate buffer (pH 2.1): methanol, 99:1 (85:15 for PTeCA[16]), at 35 °C.

The extracted pigments, corneas and synthetic melanins were also subjected to hydriodic acid hydrolysis following the protocols of Wakamatsu *et al*.[38].

Fontana-Masson histochemical staining. Fresh *Nephrotoma suturalis* eyes were prepared for sectioning by initial fixation overnight in 10% buffered formalin (4% buffered formaldehyde) at 4 °C, followed by immersion in sodium phosphate buffer, dehydration in a graded ethanol series, before clearing in xylene, and final infiltration and embedding in paraffin (Richard-Allen, Type 9). Semi-thin (5-µm) sections were then cut on a rotary ultramicrotome (LeicaRM2235), and mounted on chrome alum gelatine-coated glass microscope slides. The slides were dried overnight at 37 °C, then deparaffinised, hydrated and stained following the protocols of Carson & Cappellano[39]. Half of the sections were bleached with 10% H_2O_2 in dH_2O at room temperature for 67 h. Both bleached and unbleached sections were then stained using the Fontana-Masson method[39], but without the counterstaining step specifically required for cell nuclei. All of our slides were dehydrated and coverslips applied prior to imaging on an Olympus CX21LED microscope equipped with a digital Infinity2 camera.

Data Availability The fossil crane-flies analysed in this study are permanently accessioned into the collections of Museum Salling, Fur Museum, Fur, Denmark, and Mo-clay Museum, Nykøbing Mors,

Denmark. Our comparative trilobite fossil samples are housed in the research collections of the Department of Geology, Lund University, Lund, Sweden. All supporting data are available from the corresponding author upon reasonable request.

31. Novellino, L., Napolitano, A. & Prota, G. Isolation and characterization of mammalian eumelanins from hair and irides. *Biochim. Biophys. Acta* **1475,** 295–306 (2000).
32. Butenandt, A., Schiedt, U. & Biekert, E. Über Ommochrome, III. Mitteilung: Synthese des Xanthommatins. *Justus Liebigs Ann. Chem.* **588,** 106–116 (1954).
33. d'Ischia, M. *et al*. Melanins and melanogenesis: methods, standards, protocols. *Pigm. Cell Melanoma Res.* **26,** 616–633 (2013).
34. Thiel, V. & Sjövall, P. in *Principles and practice of analytical techniques in geosciences*. 122–170 (The Royal Society of Chemistry, 2015).
35. Lindgren, J. *et al*. Skin pigmentation provides evidence of convergent melanism in extinct marine reptiles. *Nature* **506,** 484–488 (2014).
36. Lindgren, J. *et al*. Interpreting melanin-based coloration through deep time: a critical review. *Proc. R. Soc. B* **282,** 20150614 (2015).
37. Lindgren, J. *et al*. Soft-tissue evidence for homeothermy and crypsis in a Jurassic ichthyosaur. *Nature* **564,** 359–365 (2018).
38. Wakamatsu, K., Ito, S. & Rees, J. L. The usefulness of 4-amino-3-hydroxyphenylalanine as a specific marker of pheomelanin. *Pigm. Cell Res.* **15,** 225–232 (2002).
39. Carson, F. L. & Cappellano, C. H. *Histotechnology: A Self Instructional Text* (American Society of Clinical Pathologists Press, 2015).

Supplementary Information is available in the online version of the paper.

Acknowledgements Mette Hofstedt collected FUM-N-15451, and Carsten Tell processed our extant tiger crane-fly samples. Rolf Hauff and Gareth Dyke provided comparative fossil squid ink sacs. Carina Rasmussen prepared the histological sections, performed the Fontana-Masson staining, and assisted during the TEM analysis. Financial support for this project was provided by a Swedish Research Council Grant for Distinguished Young Researchers (642-2014-3773) to J.L.

Author Contributions J.L. and D.-E.N. conceived the project. J.L., D.-E.N. and B.P.K. wrote the paper with contributions from J.R.L. and P.A., and feedback from all authors. J.L. assembled the figures with input from all authors. B.P.S., R.L.S. and H.M. prepared and curated all fossil crane-flies. J.R.L. provided comparative tiger crane-fly (*Nephrotoma*) samples. J.L. prepared the fossil thin sections, and C.A., J.L. and D.-E.N. undertook the polarized light microscopic investigation. C.A., P.S. and J.L. conducted the FEG-SEM and TEM analyses, P.L. and C.A. performed the EBSD experiments, S.I. and K.W. carried out the AHPO and HI hydrolysis analyses, P.S. and J.L. performed the ToF-SIMS experiments, M.E.E. and S.A.H. assembled the X-ray computed microtomographic data and M.E.E. made the 3D reconstructions, M.J. synthesized xanthommatin and purified both the *Nephrotoma* screening pigments and *Taeniopygia* pheomelanin, and I.R.-M. and M.J. performed the maturation experiments.

Author Information

The authors declare no competing interests.

Correspondence and requests for materials should be addressed to J.L. (johan.lindgren@geol.lu.se).

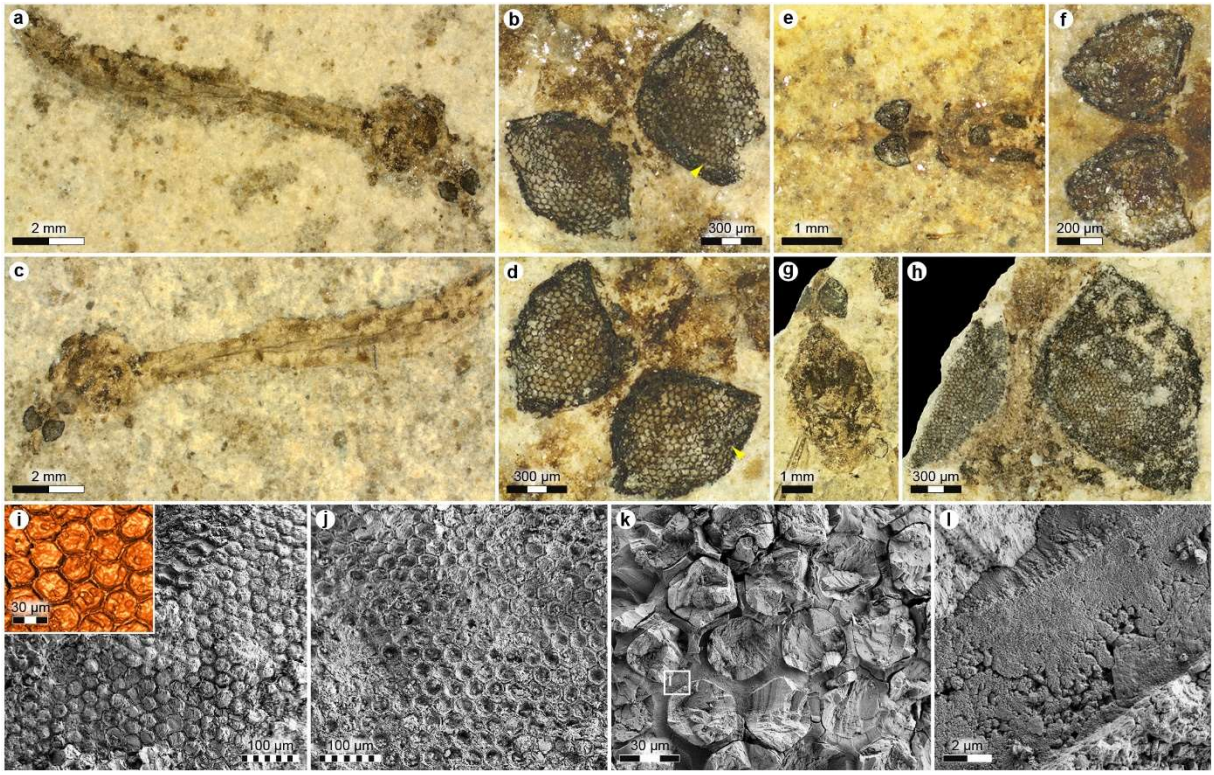

Extended Data Figure 1 | Representative samples of fossilized crane-fly compound eyes. a–**d**, Photographs (overview of specimen and enlargement of eyes, respectively) of MHM-18a, b (part and counterpart) immersed in Milli-Q water. Arrowheads in **b** and **d** indicate wrinkling along the perimeter of the optical surfaces. **e**, **f**, Photographs of MHM-18-6a (part) immersed in Milli-Q water. **g**, **h**, Photographs of FUM-N-15451 immersed in Milli-Q water (**a**–**h**; *n* = 23 fossils). **i**, FEG-SEM image and X-ray computed microtomographic rendering (inset; illustration is representative of six independently sampled data sets) of the external visual surface in FUM-N-13923 showing convex ommatidial lenses. **j**, FEG-SEM image of the internal visual surface in FUM-N-13923. Ommatidial lenses are represented by concavities. **k**, Enlargement of a transversely sectioned cornea in MHM-18-6a (for SEM-EDS element maps, see Extended Data Fig. 2). **l**, Magnification of the area demarcated in **k** showing the granular composition of the facet wall (**i**–**l**; *n* = 4). Scale bars, 2 µm (**l**), 30 µm (**i**; inset, **k**), 100 µm (**i**, **j**), 200 µm (**f**), 300 µm (**b**, **d**, **h**), 1 mm (**e**, **g**), 2 mm (**a**, **c**).

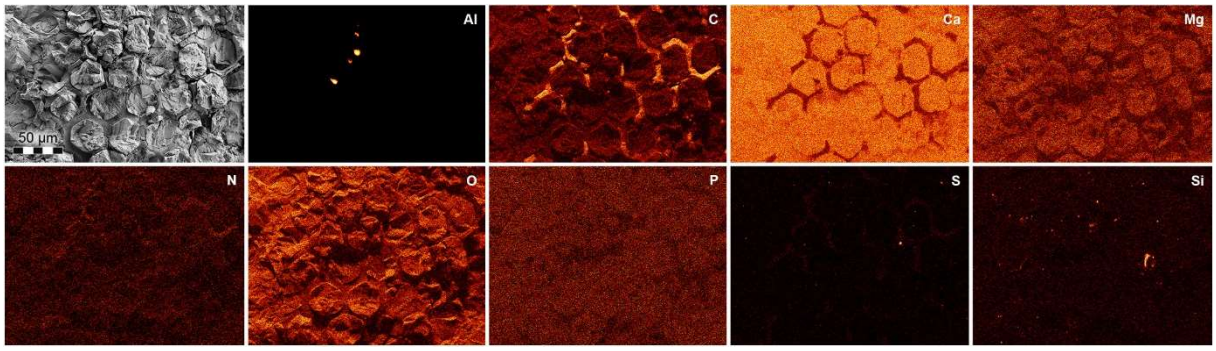

Extended Data Figure 2 | FEG-SEM micrograph and single-element EDS maps from a fossilized crane-fly compound eye (MHM-18-6a). EDS maps differentiating elevated levels of carbon with traces of nitrogen and sulfur in the corneal facet walls (identified by increased colour intensity) versus calcium and oxygen enrichment (with minor amounts of magnesium) in the ommatidial lenses. Data are representative of three independent

analyses. Al, aluminium; C, carbon; Ca, calcium; Mg, magnesium; N, nitrogen; O, oxygen; P, phosphorous; S, sulfur; Si, silicon. Scale bar, 50 µm.

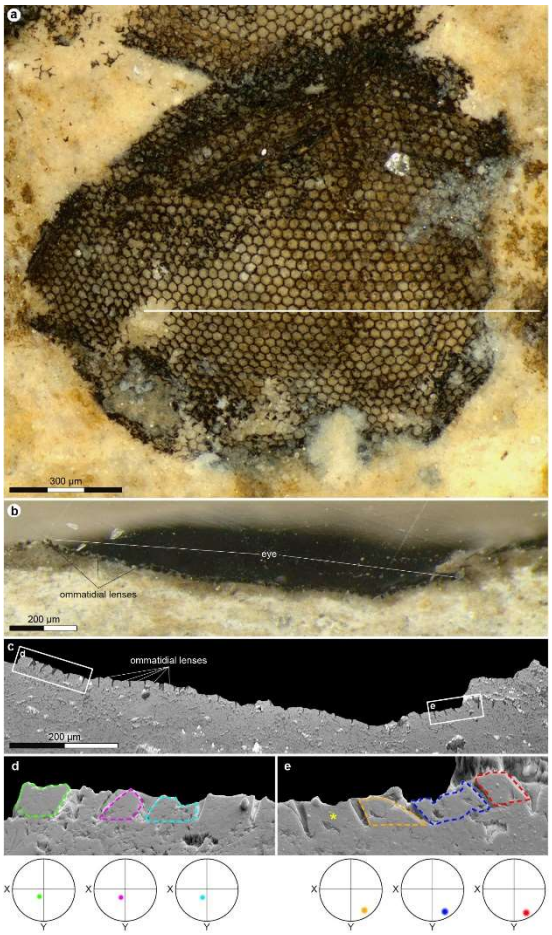

Extended Data Figure 3 | EBSD analysis of calcified crane-fly ommatidial lenses. a, Compound eye of FUM-N-13923 indicating analysed section (horizontal white line). **b**, Semi-transparent ommatidial lenses and darkly pigmented corneal facet walls shown in oblique section. **c**, FEG-SEM micrograph of the fossilized cornea. **d**, **e**, Enlargements of the boxed areas in **c**. Dashed coloured lines delineate individual ommatidial lenses analysed with EBSD (**d**, **e**; *n* = 15 separate lenses). Pole figures (stereographic projection, upper hemisphere) illustrate the {0001} (*c*-axis) orientation of six representative calcite crystals. Note that the *c*-axis is aligned with the optical axis in all lenses (yellow star = fossil lens depicted in Fig. 2c). Scale bars, 200 µm (**b**, **c**), 300 µm (**a**).

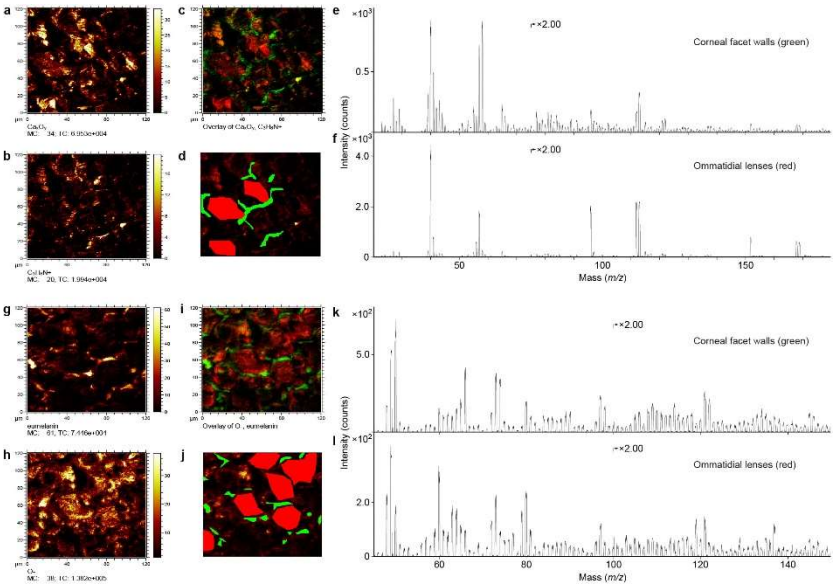

Extended Data Figure 4 | ToF-SIMS images and spectra from a fossilized crane-fly compound eye (MHM-18-6a). a–**d**, Positive ion images representing **a**, calcium carbonate (Ca_2O^+, *m/z* 96; $Ca_2O_2^+$, *m/z* 112; $Ca_2O_2H^+$, *m/z* 113; $Ca_3O_2^+$, *m/z* 152; $Ca_3O_3^+$, *m/z* 168) and **b**, a nitrogen-containing fragment ($C_3H_8N^+$, *m/z* 58), together with **c**, a two-colour overlay image of these ions where green represents the organic compound and red calcium carbonate, and **d**, the total ion image with selected regions of interest (ROIs) marked in green (corneal facet walls) and red (ommatidial lenses). **e**, **f**, Positive ion spectra generated from the ROIs indicated in **d**, representing **e**, corneal facet walls and **f**, ommatidial lenses. **g**–**j**, Images of negative ions representing **g**, eumelanin (C_4H^-, *m/z* 49; C_3N^-, *m/z* 50; C_3NO^-, *m/z* 66; C_6H^-, *m/z* 73; C_5N^-, *m/z* 74; C_8H^-, *m/z* 97) and **h**, oxygen (O^-, *m/z* 16), together with **i**, a two-colour overlay image of these ions where green represents eumelanin and red oxygen, and **j**, the total ion image with selected ROIs marked in green (corneal facet walls) and red (ommatidial lenses). **k**, **l**, Negative ion spectra generated from the ROIs indicated in **j**, representing **k**, corneal facet walls and **l**, ommatidial lenses. Data are representative of six independent measurements.

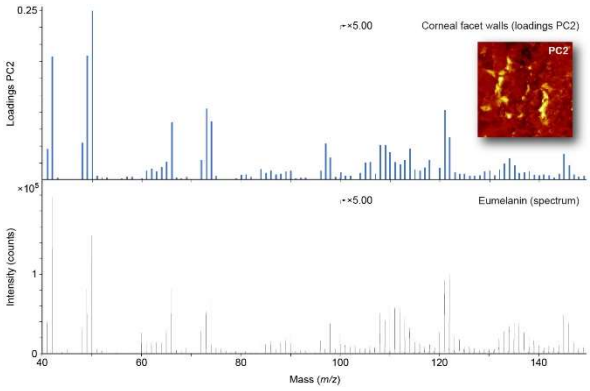

Extended data Figure 5 | Principal component analysis of ToF-SIMS images from a fossilized crane-fly compound eye. Score image of PC2 (inset) showing high scores for the corneal facet walls in MHM-18a (Fig. 3), and a diagram comparing the positive loadings for PC2 (*n* = 4 analyses) with a synthetic eumelanin reference spectrum (*n* = 6 measurements). Note close similarity between the distribution of the PC2 loadings and peak intensities in the eumelanin spectrum, indicating chemical properties of the facet walls (bright areas in the PC2 score image) directly comparable to this pigment. Negative PC2 loadings

were obtained for O^- and SiO_x^- ions representing the adjacent mineral matrix. The analyses included 141 negative ion images at nominal masses between *m/z* 10 and *m/z* 150.

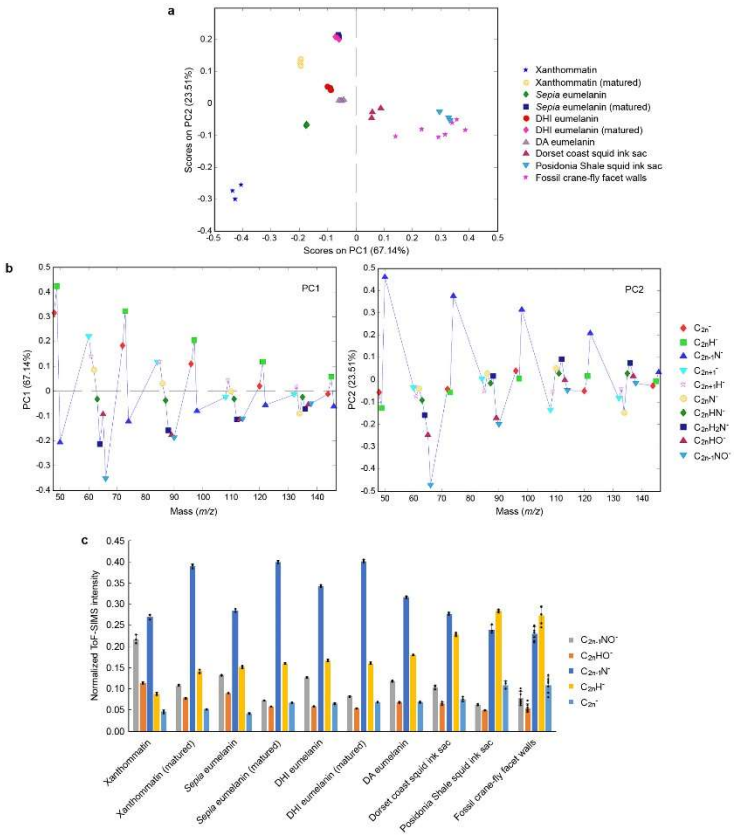

Extended data Figure 6 | Principal component analysis comparing negative ion ToF-SIMS spectra from the corneal facet walls in a fossil crane-fly with various reference materials. a, Score plot from an analysis that includes all major eumelanin peaks in the mass range *m/z* 48–146 (see Table S3) and **b**, associated loadings from PC1 and PC2 with glyphs indicating the ion categories that each peak is assigned to. **c**, Bar graph comparing the added signal intensities from all peaks in the various ion categories (error bars = +/- 1 standard deviation). **a**–**c**; Xanthommatin, *n* = 3 measurements; Xanthommatin (matured), *n* = 3 measurements; *Sepia* eumelanin, *n* = 3 measurements; *Sepia* eumelanin (matured), *n* = 3 measurements; DHI eumelanin, *n* = 3 measurements; DHI eumelanin (matured), *n* = 3 measurements; DA eumelanin, *n* = 4 measurements; Dorset coast squid ink sac, *n* = 3 measurements; Posidonia Shale squid ink sac, *n* = 3 measurements; Fossil crane-fly facet walls, *n* = 7 measurements. DA, dopamine; DHI, dihydroxyindole.

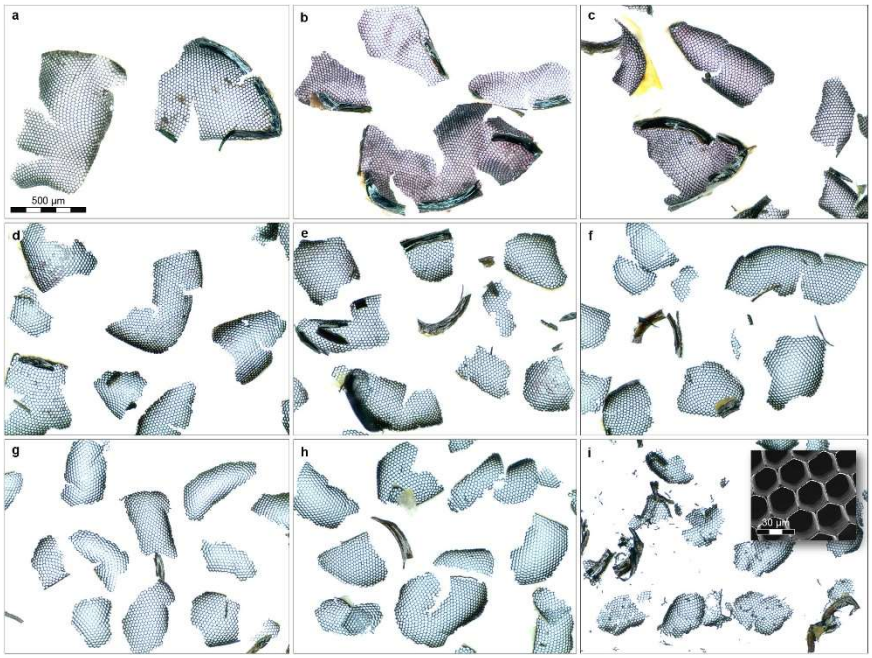

Extended Data Figure 7 | Experimentally treated *Nephrotoma suturalis* corneas. Light microscopy images showing the visual appearance of the corneas (*n* = 1,300 sampled animals) after the following sequential treatments: **a**, aqueous extraction with grinding, **b**, proteinase K and DTT (step 2; see Supplementary Information), **c**, protease and DTT (step 4), **d**, chitinase (step 5), **e**, proteinase K and DTT (step 6), **f**, chitinase (step 7), **g**, chitinase (step 9), **h**, protease and DTT (step 11), and **i**, heptane and HCl(aq). Inset shows a FEG-SEM micrograph of the isolated corneal facet walls. All experiments were repeated twice independently with similar results.

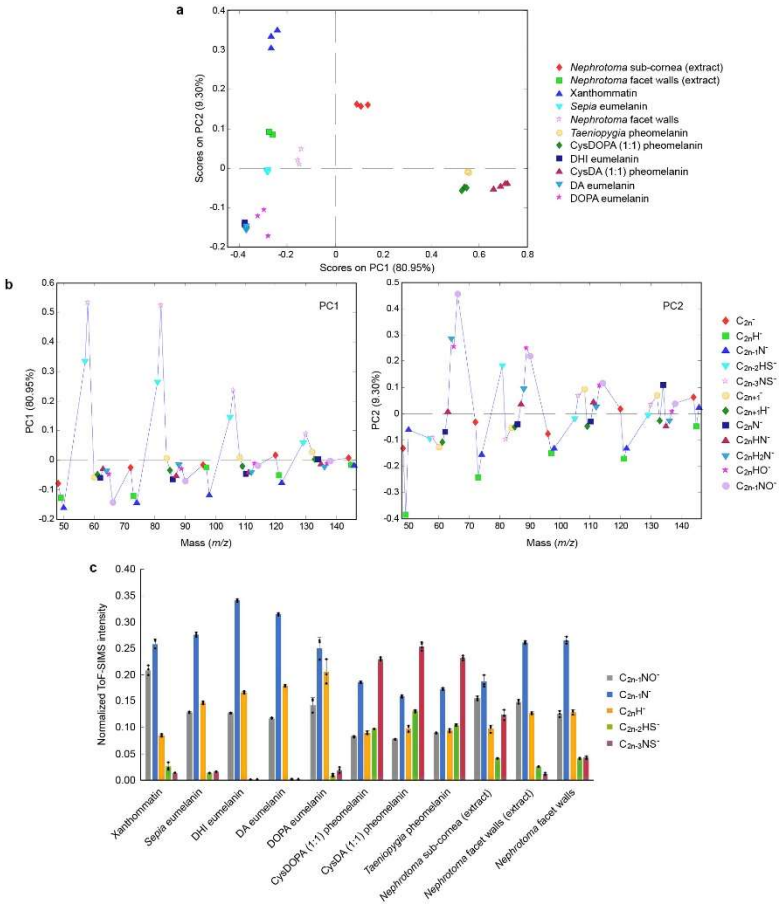

Extended data Figure 8 | Principal component analysis comparing negative ion ToF-SIMS spectra from *Nephrotoma suturalis* screening pigments with various reference materials. a, Score plot of an analysis that includes all major eumelanin and pheomelanin peaks in the mass range *m/z* 48–146 (see Table S3) and **b**, associated loadings from PC1 and PC2 with glyphs indicating the ion categories that each peak is assigned to. **c**, Bar graph comparing the added signal intensities from all peaks in the various ion categories (error bars = +/- 1 standard deviation). **a**–**c**; *Nephrotoma* sub-cornea (extract), *n* = 3 measurements; *Nephrotoma* facet walls (extract), *n* = 3 measurements; Xanthommatin, *n* = 3 measurements; *Sepia* eumelanin, *n* = 3 measurements; *Nephrotoma* facet walls, *n* = 3 measurements; *Taeniopygia* pheomelanin, *n* = 3 measurements; CysDOPA (1:1) pheomelanin, *n* = 3 measurements; DHI eumelanin, *n* = 3 measurements; CysDA (1:1) pheomelanin, *n* = 4 measurements; DA eumelanin, *n* = 4 measurements; DOPA eumelanin, *n* = 3 measurements. CysDA, cysteinyldopamine; CysDOPA, cysteinyldopa; DA, dopamine; DHI, dihydroxyindole.

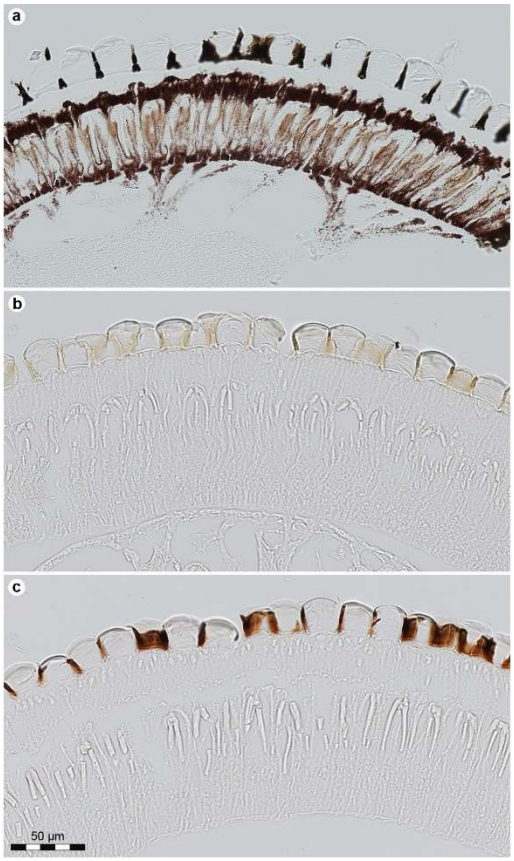

Extended Data Figure 9 | Histological sections through *Nephrotoma suturalis* compound eyes stained with Fontana-Masson. a, Untreated section. **b**, Section bleached with hydrogen peroxide. **c**, Bleached section stained with Fontana-Masson. Note darkening of the corneal cuticle in the facet walls, indicating presence of melanin. Images are representative of three independent experiments.

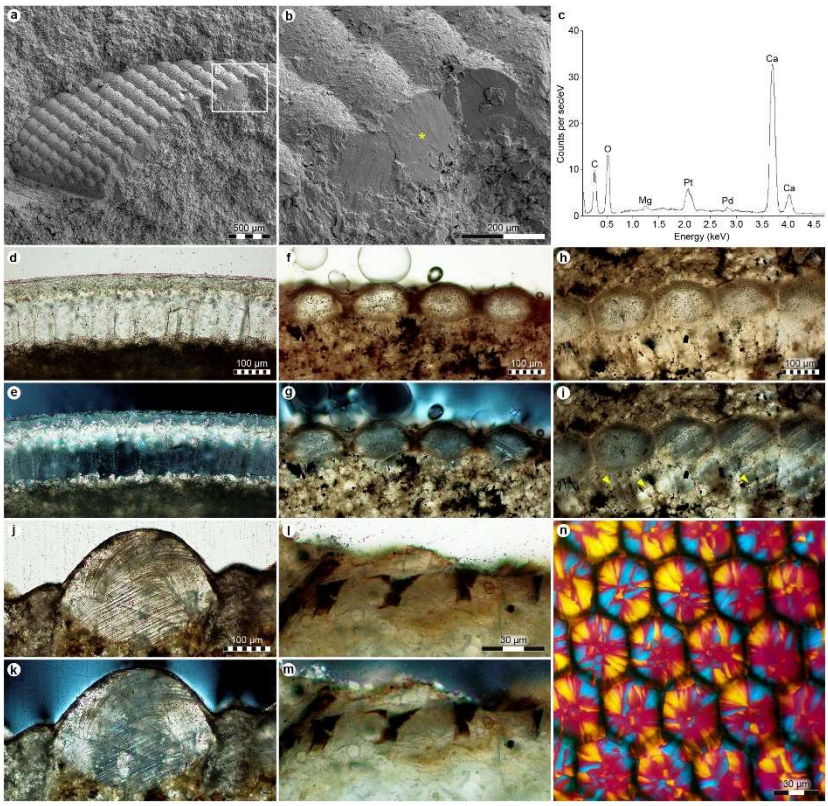

Extended Data Figure 10 | FEG-SEM and polarized light micrographs of trilobite, fossil crane-fly and extant decapod ommatidial lenses. **a**, FEG-SEM micrograph of a holochroal eye (LO 12437t) of the trilobite *Telephina bicuspis* (Middle Ordovician, Norway). **b**, Enlargement of fractured ommatidial lenses (**a**, **b**; *n* = 3 fossils). **c**, Single spot EDS spectrum acquired from the lens marked by a yellow star in **b** showing carbon, oxygen and calcium intensities consistent with calcite (compare Fig. 2b). Platinum and palladium peaks derive from the sample pre-treatment (coating). Data are representative of six independent measurements. **d**, Plane-polarized light microscopy section through a holochroal eye (LO 12439t) of the trilobite *Nileus armadillo* (Middle Ordovician, Sweden). **e**, Equivalent cross-polarized light micrograph. **f**, Plane-polarized light microscopy section through ommatidial lenses in an eye (LO 12438t) of *T. bicuspis*. **g**, Equivalent cross-polarized light micrograph. **h**, Plane-polarized light microscopy section through a second eye (LO 12437t) of *T. bicuspis*. **i**, Equivalent cross-polarized light micrograph showing calcite crystal growth beyond the preserved lenses (arrowheads; see Supplementary Information). **j**, Plane-polarized light microscopy section through an ommatidial lens in a schizochroal eye (LO 12440t) of the trilobite *Phacops latifrons* (Middle Devonian, Germany). **k**, Equivalent cross-polarized light micrograph. **l**, Plane-polarized light microscopy section through ommatidial lenses in an eye of a fossil crane-fly (FUM-N-13923). **m**, Equivalent cross-polarized light micrograph. Data in **d**–**m** are representative of three independent analyses. **n**, Cross-polarized light micrograph of calcite crystals in a compound eye of the extant sandy swimming crab, *Liocarcinus depurator* (*n* = 3 specimens). Scale bars, 30 µm (**l**, **n**), 100 µm (**d**, **f**, **h**, **j**), 200 µm (**b**), 500 µm (**a**).